Methane Storage Hot Paper

International Edition: DOI: 10.1002/anie.201511006
German Edition: DOI: 10.1002/ange.201511006

A Metal–Organic Framework with a Pore Size/Shape Suitable for Strong Binding and Close Packing of Methane

Jiao-Min Lin, Chun-Ting He, Yan Liu, Pei-Qin Liao, Dong-Dong Zhou, Jie-Peng Zhang,* and Xiao-Ming Chen*

Dedicated to Professor Thomas C. W. Mak on the occasion of his 80th birthday

Abstract: *Much effort has been devoted to develop new porous structures for methane storage. We report a new porous coordination framework showing exceptional methane uptakes (e.g. 263 v/v at 298 K and 65 bar) and adsorption enthalpies (21.6 kJ mol^{-1}) as high as current record holders functionalized by open metal sites. Computational simulations demonstrated that the hierarchical pore structure consisting of single-wall nanocages has suitable sizes/shapes and organic binding sites to enforce not only strong host–methane and methane–methane interactions but also dense packing of methane molecules.*

Methane (natural gas) is an attractive petroleum replacement for fueling automobiles, but its storage for transportation applications still remains a challenge because of its low volumetric energy density under standard conditions.[1] Compared with conventional liquefaction and compression methods, physical adsorption of methane within porous materials is a more potentially useful approach in terms of both cost and safety concerns.

The large pore volumes and surface areas, and designable pore surface structures of porous coordination polymers (PCPs) or metal–organic frameworks (MOFs)[2] are intriguing for physical adsorption of methane.[3] Because it is easy for MOFs to provide sufficiently large surface areas and pore volumes, the main research is focused on improving the methane binding affinity, usually by introducing open metal sites (OMSs).[4] Indeed, among various adsorbents,[3,5] the highest volumetric methane uptakes (e.g., 202–230 cm^3(STP) cm^{-3} at 35 bar, 239–267 cm^3(STP) cm^{-3} at 65 bar) at room temperature are held by several MOFs functionalized by OMSs, such as HKUST-1,[3e] UTSA-76a,[5e] Ni-MOF-74,[3d] and PCN-14.[3d] However, the concentration of OMSs can be hardly improved, even when the undesired increase of adsorbent weight is not considered.[6] Other approaches have also been used to optimize methane adsorption performance, but they are generally less effective than for OMSs.[3b,7] For example, the highest volumetric methane uptakes reported so far for OMS-free MOFs at 298 K and 65 bar are only 214–215 cm^3(STP) cm^{-3}.[3d,5f]

Besides the host–methane interactions, methane–methane interactions can also contribute to methane adsorption.[5g] However, pure methane–methane interactions are too weak (the vaporization enthalpy of methane is only about 8 kJ mol^{-1}) for achieving high methane uptake at ambient conditions, as exemplified by the poor methane-storage performances of large-pore adsorbents.[5j] Therefore, developing new porous structures with novel methane binding sites, and suitable pore sizes/shapes that can maximize host–methane and methane–methane cooperation should be a research target. In this work, we report very high methane adsorption capacity and novel adsorption mechanism observed in a new OMS-free MOF possessing a novel pore structure.

Colorless prismatic crystals of $[Zn_3(pypz)_3(btc)]\cdot$guest (MAF-38 or **1·g**, Hpypz = 4-(1*H*-pyrazol-4-yl)pyridine, H_3btc = 1,3,5-benzenetricarboxylic acid) were obtained by solvothermal reaction. Single-crystal X-ray diffraction for **1·g** revealed a three-dimensional (3D) non-interpenetrated coordination network crystallizing in the high-symmetry trigonal space group *R*-3 (Table S1). The asymmetric unit of **1·g** contains one Zn^{II} ion, one pypz$^-$, and one third of a btc^{3-} ligand. The Zn^{II} ion coordinates with one pyridyl and two pyrazolate nitrogen donors from three different pypz$^-$ ligands, as well as a semi-chelating carboxylate group from the btc^{3-} ligand in a geometry between tetrahedral and square-pyramidal (Figure S1 in the Supporting Information). Two Zn^{II} ions are bridged by two bidentate pyrazolate moieties to form a binuclear $Zn_2(Rpy)_2(Rpz)_2(RCOO)_2$ unit (Rpy = pyridyl group, Rpz$^-$ = pyrazolate group, RCOO$^-$ = carboxylate group). The pypz$^-$ and btc^{3-} ligands connect two and three $Zn_2(py)_2(pz)_2(RCOO)_2$ units, respectively. Regarding btc^{3-} as a 3-connected node, $Zn_2(py)_2(pz)_2(RCOO)_2$ as a 6-connected node, and pypz$^-$ as a linker, respectively, **1** can be simplified as a non-interpenetrated 3D (3,6)-connected network (Figure S2).[8]

The coordination framework of **1** can be also regarded as a packing of small octahedral cages and large quasi-cuboctahedral cages in the ratio of 1:1, which are both squashed along the *c*-axis (Figure S3). The small cage is enclosed by six $Zn_2(py)_2(pz)_2(RCOO)_2$ units, six pypz$^-$, and two btc^{3-} ligands, with internal free diameters of approximately 6.2 and 8.6 Å

[*] Dr. J.-M. Lin, C.-T. He, Y. Liu, P.-Q. Liao, D.-D. Zhou, Prof. Dr. J.-P. Zhang, Prof. Dr. X.-M. Chen
MOE Key Laboratory of Bioinorganic and Synthetic Chemistry
School of Chemistry and Chemical Engineering
Sun Yat-Sen University, Guangzhou 510275 (China)
E-mail: zhangjp7@mail.sysu.edu.cn
hechunt@mail2.sysu.edu.cn

Supporting information and the ORCID identification number(s) for the author(s) of this article can be found under http://dx.doi.org/10.1002/anie.201511006.

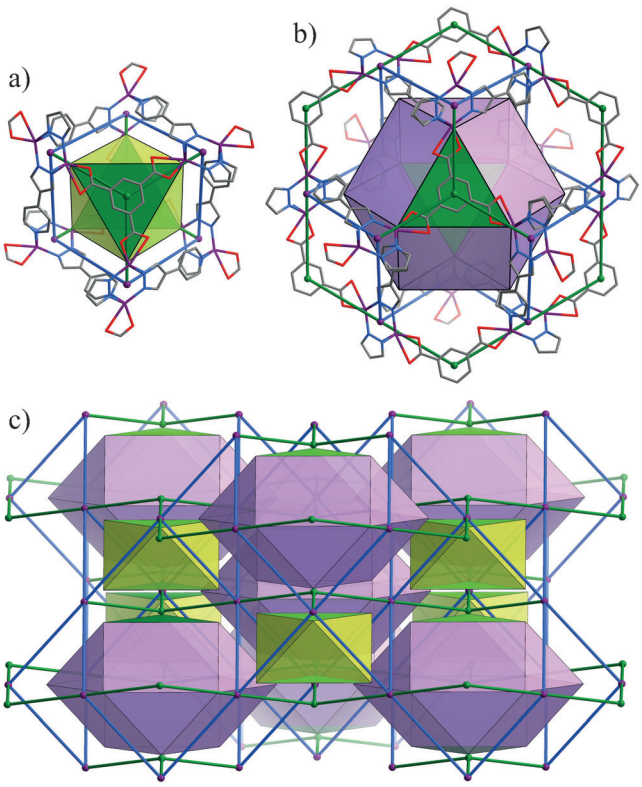

Figure 1. Perspective views of the a) small octahedral cage, b) large quasi-cuboctahedral cage, and c) simplified cage-based structure of **1**. Atom colors: Zn violet, C gray, N blue, O red.

along the *c*-axis and across the *ab*-plane, respectively (Figure 1a). In this cage, six vertices are occupied by the $Zn_2(py)_2(pz)_2(RCOO)_2$ units, and two axial trigonal faces are blocked by the btc^{3-} ligands, whereas the other six equatorial ones have window diameters of around 4.0–4.8 Å. The large cage consists of six $Zn_2(py)_2(pz)_2(RCOO)_2$ units, six isophthalate moieties from six btc^{3-}, two complete btc^{3-}, and twelve $pypz^-$ ligands, with internal free diameters of approximately 9.0 and 14.2 Å along the *c*-axis and across the *ab*-plane, respectively (Figure 1b). For this cage, two axial trigonal faces are also blocked by two btc^{3-} ligands, while other six trigonal and six quadrangular faces have window diameters of approximately 4.0–4.8 and 4.0–7.2 Å, respectively. Each large cage connects with six neighboring ones through sharing the quadrangular faces, forming a 6-connected **pcu**-type 3D intersecting channel. The small and large cages are also interconnected by sharing their six open trigonal faces, leading to a 3D hierarchical pore system (Figure 1c). Since all the blocked faces and edges of these nanocages are constructed by thin walls (as thick as a carbon atom), **1** exhibits large solvent-accessible void ratio of 65.1% (calculated by Platon using probe radius of 1.2 Å) and low crystallography density of 0.761 $g\,cm^{-3}$, corresponding to a theoretical pore volume of 0.855 $cm^3\,g^{-1}$.

Thermogravimetry and variable-temperature powder X-ray diffraction showed that **1**·**g** can be readily activated by exchanging the guest with CH_3OH and then heating at 120 °C, and that guest-free **1** is stable up to 350 °C (Figures S4,S5).

The porosity of **1** was evaluated by N_2 sorption isotherm at 77 K, which exhibits the type-I character with a saturated uptake of 517 $cm^3(STP)\,g^{-1}$, giving a pore volume of 0.808 $cm^3\,g^{-1}$ or 0.615 $cm^3\,cm^{-3}$ (Figure S6). For comparison, a grand canonical Monte Carlo (GCMC) simulation gave a saturated N_2 uptake of 523 $cm^3(STP)\,g^{-1}$, which confirmed that the sample used for sorption measurement possessed high crystallinity/purity and its density should be similar with the crystallography value. The Brunauer–Emmett–Teller (BET) and Langmuir surface areas were calculated to be 2022 and 2229 $m^2\,g^{-1}$, respectively. It is interesting that the pore sizes/shapes (Figure S3), pore volumes, and surface areas of **1** and PCN-14 are quite similar (Tables S2,S3).[3d,5h]

To evaluate the methane-storage performance of **1**, high-pressure excess adsorption isotherms were measured at 298 K and repeated three times (Figures 2 and Figures S7,S8), and then empirically transformed to total adsorption isotherms.

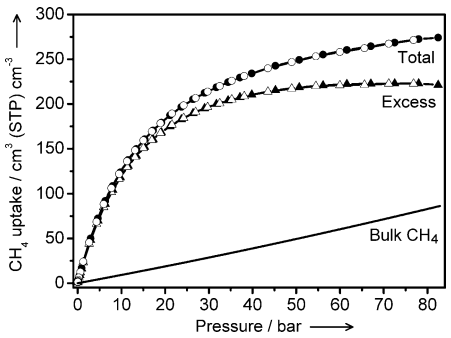

Figure 2. Total and excess methane adsorption (solid) and desorption (open) isotherms of **1** at 298 K.

The total methane uptake of **1** reaches 4.5, 13.3, 15.4, and 16.0 $mmol\,g^{-1}$ at 5, 35, 65, and 80 bar, respectively, corresponding to 7.1, 21.2, 24.7, and 25.6 wt% or 76, 226, 263, and 273 $cm^3(STP)\,cm^{-3}$ (Figure 2). The working capacity, defined as the difference in total uptakes between the lower limit pressure of 5 bar for driving an internal combustion engine and a higher pressure such as 35, 65, and 80 bar, are 14.1, 17.6, and 18.5 wt% or 150, 187, and 197 $cm^3(STP)\,cm^{-3}$, respectively.

Compared with the best performing MOFs (Table S2), the volumetric methane uptakes of **1** at all measured pressures are similar with the current record holder HKUST-1,[3e] and much higher than for other MOFs, except for PCN-14 and Ni-MOF-74 at very low pressures such as 5 bar.[3d] The volumetric working capacity of **1** is also similar with HKUST-1, higher than for most other MOFs including PCN-14 and Ni-MOF-74, and only slightly lower than several MOFs possessing framework flexibility or very large pore volumes/surface areas.[5b–e] From the gravimetric point of view (Table S3), the methane-storage performance of **1** is still high especially at 35 bar and lower pressures, but lower than for some MOFs showing very low crystal densities and very large pore volumes/surface areas.[5c–f] It should be noted that, while the volumetric uptake reflects more the binding strength and space utilization efficiency, the gravimetric uptake is more relevant with the

atomic weights of the framework components. Considering that adsorption affinity, surface area, and pore volume play the most important roles at low, medium, and high pressures, respectively, the high methane storage performances of **1** especially at 35 bar indicate strong methane binding and efficient utilization of its pores.

The coverage-dependent CH_4 adsorption enthalpy (Q_{st}) of **1** was calculated with the Clausius–Clapeyron equation using isotherms measured at 273, 288, and 298 K, which could be well described by the Langmuir–Freundlich model (Figures 3 and Figure S9,S10). At zero coverage, Q_{st} was calculated to be 21.6 ± 1.8 kJ mol^{-1}, which is among the highest

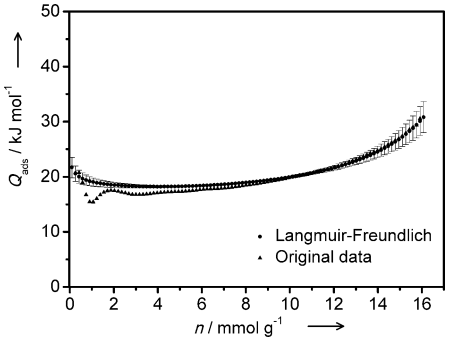

Figure 3. Coverage-dependent CH_4 adsorption enthalpy profiles (calculated by two methods) of **1**.

reported values and similar with that of Ni-MOF-74 (21.4 kJ mol^{-1}) which has strong OMSs.[3b,e] When the CH_4 coverage increases, Q_{st} decreases slowly to 18.2 ± 0.2 kJ mol^{-1} at 3.65 mmol g^{-1}, and then slowly increases to 30.8 ± 2.8 kJ mol^{-1} at 16.1 mmol g^{-1}.

The methane adsorption mechanism of **1** was studied by GCMC simulations and periodic density functional theory (PDFT) optimizations. As shown in Figure S11, the GCMC simulated isotherm is in good agreement with the measured one. By performing a site-by-site search, a series of strong adsorption sites were found. The trigonal window connecting the small and large cages serves as the primary adsorption site for CH_4 with a high binding energy of 28.2 kJ mol^{-1} (Figure 4a), in which the CH_4 molecule roughly match the pore size/shape with multiple host–guest contacts including C–H···O and C–H···N hydrogen bonds, as well as C–H···π interactions. The secondary and ternary CH_4 adsorption sites locate at the quadrangular window connecting the large cages (Figure 4b) and the top of the carboxylate group of the btc^{3-} ligand inside the small cage (Figure 4c), showing binding energies of 25.8 and 25.6 kJ mol^{-1}, respectively. However, the CH_4 molecules at the secondary and ternary sites interact with not only the host framework but also the CH_4 molecules previously adsorbed at the primary site. Without the CH_4 molecules at the primary site, the binding energies of the secondary and ternary sites would decrease to 24.9 and 21.8 kJ mol^{-1}, respectively. Interestingly, two and six crystallographically equivalent CH_4 molecules at the secondary and ternary adsorption sites form supramolecular dimer (Figure 4b) or cage-like cluster (Figure 4c), further increasing the

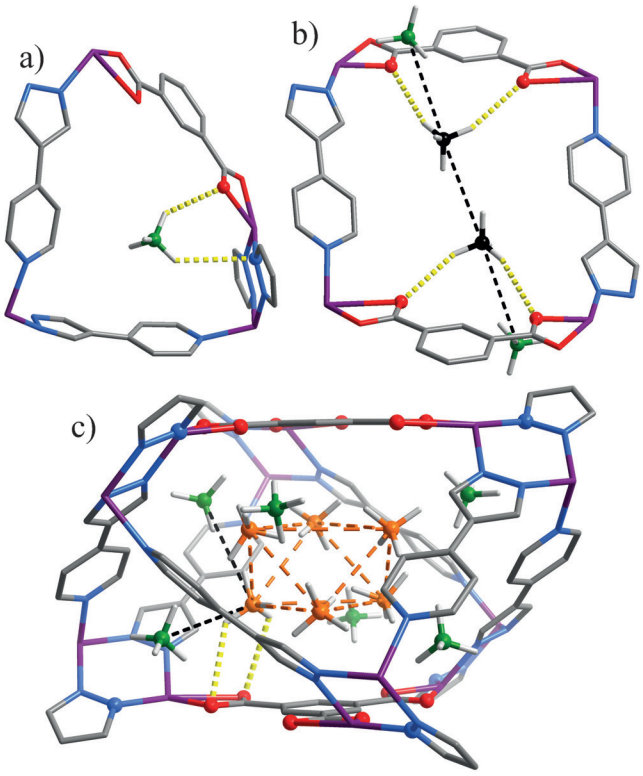

Figure 4. The a) primary (green), b) secondary (black), and c) ternary (orange) CH_4 adsorption sites, as well as the unique supramolecular CH_4 dimer and hexamer in **1**, as revealed by computational simulation. Dashed lines represent host–guest C···O/N (yellow) and guest–guest C···C (other colors) interactions shorter than 5 Å (See Table S4 for detailed data).

binding energies of these sites to 27.0 and 28.7 kJ mol^{-1}, respectively.

Later adsorption sites locate in the large cage with a smaller pore confinement effect (Figure S12). Nevertheless, they also exhibit similar host–guest and guest–guest interactions to those of the secondary and ternary sites, maintaining the binding energy at 28 kJ mol^{-1} at loading above 400 cm^3(STP) cm^{-3} (Table S4). Only the last adsorption site (3 CH_4 molecules per unit cell) is completely surrounded by previously adsorbed CH_4 molecules, but by virtue of very suitable CH_4···CH_4 interactions, the binding energy is still 22.4 kJ mol^{-1}. During the entire simulation process, each CH_4 molecule can be adsorbed without needing to move previously adsorbed molecules, and the final saturated adsorption structure has 129 CH_4 molecules per unit cell (25.7 mmol g^{-1}, 41.1 wt %, or 438 cm^3(STP) cm^{-3}). Inside the pore (65.1 %), there is a CH_4 packing density of 0.481 g cm^{-3} even higher than that of liquid methane (0.423 g cm^{-3}). Although this density can be only possibly achieved at lower temperatures and/or higher pressures, it highlights the suitable pore sizes/shapes of **1** for close packing of methane and encourages further development of strong methane binding sites.

For comparison, we used the same methods to simulate CH_4 adsorption on MOF-5[2j] and PCN-14,[5h] which have similar high-symmetry hierarchical cage-based pore structures and similar/larger pore volumes and surface areas, but

significantly or slightly different pore sizes/shapes compared with **1** (Figure S3). As shown in Figures S13–S15 and Tables S5,S6, CH_4 molecules adsorbed in MOF-5/PCN-14 pack in relatively loose configurations, and can only achieve packing densities much lower than that of liquid methane. Structural examination of their simulated host–guest structures showed that the adsorbed CH_4 molecules can hardly interact simultaneously with the host framework and other CH_4 molecules, being consistent with their relatively low and/or sharply decreased adsorption enthalpies.

In summary, we show that very high methane adsorption capacity can be achieved by an OMS-free MOF, in which the pore size/shape and strong organic binding sites synergistically reinforce host–guest and guest–guest interactions to give exceptionally high adsorption enthalpy and efficient utilization of the pore space. These results may shed some light on developing new adsorbent materials for gas-storage applications.

Experimental Section

MAF-38 (**1**·**g**): A mixture of $Zn(NO_3)_2{\cdot}6H_2O$ (0.089 g, 0.3 mmol), Hpypz (0.052 g, 0.36 mmol), H_3btc (0.021 g, 0.1 mmol), and *N*,*N*-dimethylformamide (DMF, 6 mL) was sealed in a 10-mL Teflon-lined stainless-steel container and kept at 140 °C for 3 days, then cooled to room temperature at a rate of 5 °C h^{-1}. Colorless prismatic crystals were obtained with the yield of 82 % based of Zn. Elemental analysis calcd. (%) for $[Zn_3(pypz)_3(btc)]{\cdot}6DMF{\cdot}12H_2O$ ($Zn_3O_{24}N_{15}C_{51}H_{87}$): C 41.09, H 5.88, N 14.09; found: C 41.42, H 5.58, N 13.92.

High-pressure excess methane adsorption isotherms in the range of 0–80 bar were measured with an automatic volumetric sorption apparatus (BELSORP-HP). The measurement temperatures were controlled by a computer-controlled water bath or an ice-water bath. Ultrahigh-purity He was used to determine the dead space of the sample cell. The adsorption data were corrected to give the final gravimetric excess adsorption isotherm $n_{ex}(P,T)$, by subtracting the background adsorption measured with the empty sample cell using the same test parameters. The total adsorption, which represents the real gas-storage performance of the porous material but cannot be directly measured, was calculated by [Eq. (1)]:

$$n_{tot}(P,T) = n_{ex}(P,T) + \rho_{gas}(P,T) \times V_p \quad (1)$$

Where $\rho_{gas}(P,T)$ is the density of bulk methane at pressure P and temperature T, and V_p is the pore volume of the porous material determined from N_2 adsorption isotherm at 77 K. The volumetric isotherms were obtained by multiplying the gravimetric isotherms with the crystallography density of the host framework.

Note that pore volume measurement is crucial for the above method. When V_p is larger than the theoretical values, the sample can have hollow defect and/or undergone framework expansion, meaning that the sample density is lower than the crystallographic density.

Acknowledgements

This work was supported by the "973 Project" (2014CB845602 and 2012CB821706) and NSFC (21225105, 21290173, and 21473260).

Keywords: adsorption · host–guest interactions · guest–guest interactions · metal–organic frameworks · methane

How to cite: *Angew. Chem. Int. Ed.* **2016**, *55*, 4674–4678
Angew. Chem. **2016**, *128*, 4752–4756

[1] a) R. F. Cracknell, P. Gordon, K. E. Gubbins, *J. Phys. Chem. C* **1993**, *97*, 494–499; b) V. C. Menon, S. Komarneni, *J. Porous Mater.* **1998**, *5*, 43–58.

[2] a) Y. Yan, I. Telepeni, S. Yang, X. Lin, W. Kockelmann, A. Dailly, A. J. Blake, W. Lewis, G. S. Walker, D. R. Allan, S. A. Barnett, N. R. Champness, M. Schröder, *J. Am. Chem. Soc.* **2010**, *132*, 4092–4094; b) D. Liu, H. Wu, S. Wang, Z. Xie, J. Li, W. Lin, *Chem. Sci.* **2012**, *3*, 3032–3037; c) R. K. Motkuri, H. V. R. Annapureddy, M. Vijaykumar, H. T. Schaef, P. F. Martin, B. P. McGrail, L. X. Dang, R. Krishna, P. K. Thallapally, *Nat. Commun.* **2014**, *5*, 4368; d) J. Y. Lee, L. Pan, X. Huang, T. J. Emge, J. Li, *Adv. Funct. Mater.* **2011**, *21*, 993–998; e) M. Eddaoudi, J. Kim, N. Rosi, D. Vodak, J. Wachter, M. O'Keeffe, O. M. Yaghi, *Science* **2002**, *295*, 469–472; f) N. M. Padial, E. Quartapelle Procopio, C. Montoro, E. López, J. E. Oltra, V. Colombo, A. Maspero, N. Masciocchi, S. Galli, I. Senkovska, S. Kaskel, E. Barea, J. A. R. Navarro, *Angew. Chem. Int. Ed.* **2013**, *52*, 8290–8294; *Angew. Chem.* **2013**, *125*, 8448–8452; g) P. Horcajada, F. Salles, S. Wuttke, T. Devic, D. Heurtaux, G. Maurin, A. Vimont, M. Daturi, O. David, E. Magnier, N. Stock, Y. Filinchuk, D. Popov, C. Riekel, G. Férey, C. Serre, *J. Am. Chem. Soc.* **2011**, *133*, 17839–17847; h) R. Matsuda, R. Kitaura, S. Kitagawa, Y. Kubota, R. V. Belosludov, T. C. Kobayashi, H. Sakamoto, T. Chiba, M. Takata, Y. Kawazoe, Y. Mita, *Nature* **2005**, *436*, 238–241; i) B. Zheng, J. Bai, J. Duan, L. Wojtas, M. J. Zaworotko, *J. Am. Chem. Soc.* **2011**, *133*, 748–751; j) H. Li, M. Eddaoudi, M. O'Keeffe, O. M. Yaghi, *Nature* **1999**, *402*, 276–279.

[3] a) T. A. Makal, J.-R. Li, W. Lu, H.-C. Zhou, *Chem. Soc. Rev.* **2012**, *41*, 7761–7779; b) Y. He, W. Zhou, G. Qian, B. Chen, *Chem. Soc. Rev.* **2014**, *43*, 5657–5678; c) K. Konstas, T. Osl, Y. Yang, M. Batten, N. Burke, A. J. Hill, M. R. Hill, *J. Mater. Chem.* **2012**, *22*, 16698–16708; d) J. A. Mason, M. Veenstra, J. R. Long, *Chem. Sci.* **2014**, *5*, 32–51; e) Y. Peng, V. Krungleviciute, I. Eryazici, J. T. Hupp, O. K. Farha, T. Yildirim, *J. Am. Chem. Soc.* **2013**, *135*, 11887–11894; f) X.-S. Wang, S. Ma, K. Rauch, J. M. Simmons, D. Yuan, X. Wang, T. Yildirim, W. C. Cole, J. J. López, A. de Meijere, H.-C. Zhou, *Chem. Mater.* **2008**, *20*, 3145–3152; g) C. Song, Y. Ling, Y. Feng, W. Zhou, T. Yildirim, Y. He, *Chem. Commun.* **2015**, *51*, 8508–8511.

[4] a) H. Wu, W. Zhou, T. Yildirim, *J. Am. Chem. Soc.* **2009**, *131*, 4995–5000; b) Z. Guo, H. Wu, G. Srinivas, Y. Zhou, S. Xiang, Z. Chen, Y. Yang, W. Zhou, M. O'Keeffe, B. Chen, *Angew. Chem. Int. Ed.* **2011**, *50*, 3178–3181; *Angew. Chem.* **2011**, *123*, 3236–3239; c) H. Wu, J. M. Simmons, Y. Liu, C. M. Brown, X.-S. Wang, S. Ma, V. K. Peterson, P. D. Southon, C. J. Kepert, H.-C. Zhou, T. Yildirim, W. Zhou, *Chem. Eur. J.* **2010**, *16*, 5205–5214.

[5] a) C. M. Simon, J. Kim, D. A. Gomez-Gualdron, J. S. Camp, Y. G. Chung, R. L. Martin, R. Mercado, M. W. Deem, D. Gunter, M. Haranczyk, D. S. Sholl, R. Q. Snurr, B. Smit, *Energy Environ. Sci.* **2015**, *8*, 1190–1199; b) J. A. Mason, J. Oktawiec, M. K. Taylor, M. R. Hudson, J. Rodriguez, J. E. Bachman, M. I. Gonzalez, A. Cervellino, A. Guagliardi, C. M. Brown, P. L. Llewellyn, N. Masciocchi, J. R. Long, *Nature* **2015**, *527*, 357–361; c) B. Li, H.-M. Wen, H. Wang, H. Wu, T. Yildirim, W. Zhou, B. Chen, *Energy Environ. Sci.* **2015**, *8*, 2504–2511; d) D. Alezi, Y. Belmabkhout, M. Suyetin, P. M. Bhatt, Ł. J. Weseliński, V. Solovyeva, K. Adil, I. Spanopoulos, P. N. Trikalitis, A.-H. Emwas, M. Eddaoudi, *J. Am. Chem. Soc.* **2015**, *137*, 13308–13318; e) B. Li, H.-M. Wen, H. Wang, H. Wu, M. Tyagi, T. Yildirim, W. Zhou, B. Chen, *J. Am. Chem. Soc.* **2014**, *136*, 6207–6210; f) F. Gándara, H. Furukawa, S. Lee, O. M. Yaghi, *J. Am. Chem. Soc.* **2014**, *136*, 5271–5274; g) Z. Hulvey, B. Vlaisavljevich, J. A. Mason, E. Tsivion, T. P. Dougherty, E. D. Bloch, M. Head-Gordon, B. Smit, J. R. Long, C. M. Brown, *J. Am. Chem. Soc.* **2015**, *137*, 10816–10825; h) S. Ma, D.

Sun, J. M. Simmons, C. D. Collier, D. Yuan, H.-C. Zhou, *J. Am. Chem. Soc.* **2008**, *130*, 1012 – 1016; i) M. Kondo, T. Yoshitomi, H. Matsuzaka, S. Kitagawa, K. Seki, *Angew. Chem. Int. Ed. Engl.* **1997**, *36*, 1725 – 1727; *Angew. Chem.* **1997**, *109*, 1844 – 1846; j) D. A. Gomez-Gualdron, O. V. Gutov, V. Krungleviciute, B. Borah, J. E. Mondloch, J. T. Hupp, T. Yildirim, O. K. Farha, R. Q. Snurr, *Chem. Mater.* **2014**, *26*, 5632 – 5639; k) I. Spanopoulos, C. Tsangarakis, E. Klontzas, E. Tylianakis, G. Froudakis, K. Adil, Y. Belmabkhout, M. Eddaoudi, P. N. Trikalitis, *J. Am. Chem. Soc.* **2016**, *138*, 1568 – 1574.

[6] Z. Zhang, Y. Zhao, Q. Gong, Z. Li, J. Li, *Chem. Commun.* **2013**, *49*, 653 – 661.

[7] a) Y. He, W. Zhou, T. Yildirim, B. Chen, *Energy Environ. Sci.* **2013**, *6*, 2735 – 2744; b) G. Barin, V. Krungleviciute, D. A. Gomez-Gualdron, A. A. Sarjeant, R. Q. Snurr, J. T. Hupp, T. Yildirim, O. K. Farha, *Chem. Mater.* **2014**, *26*, 1912 – 1917; c) L. D. Tran, J. I. Feldblyum, A. G. Wong-Foy, A. J. Matzger, *Langmuir* **2015**, *31*, 2211 – 2217.

[8] a) C.-K. Tan, J. Wang, J.-D. Leng, L.-L. Zheng, M.-L. Tong, *Eur. J. Inorg. Chem.* **2008**, 771 – 778; b) F. A. Mautner, L. Öhrström, B. Sodin, R. Vicente, *Inorg. Chem.* **2009**, *48*, 6280 – 6286.

Received: November 26, 2015
Revised: February 18, 2016
Published online: March 4, 2016

